# Ion drag effects in inductively coupled plasmas for etching

Wenli Z. Collison[a] and Mark J. Kushner[b]
*University of Illinois, Department of Electrical and Computer Engineering, Urbana, Illinois 61801*

(Received 5 September 1995; accepted for publication 22 November 1995)

Ion drag refers to Coulomb momentum transfer collisions between a directed flux of charged particles and a second charged species. It is an important force in determining the motion of negatively charged dust particles in plasma processing reactors. The same ion drag mechanism acts between the directed flux of positive ions moving towards the boundaries of a plasma etching reactor and negative ions being accelerated by electrostatic forces towards the center of the plasma. In this letter, we discuss the parameter space for inductively coupled plasma etching reactors in which ion drag forces on negative ions influence their transport using results from a two-dimensional plasma equipment model. We find that ion drag forces on negative ions are important at high plasma densities and low ion temperatures. Under these conditions, the large positive ion flux, coupled with a large Coulomb cross section, creates an ion drag force which may dominate the electrostatic forces on negative ions. The end result is that negative ions may accumulate near the sheath edge. © *1996 American Institute of Physics.* [S0003-6951(96)04105-5]

It is a well-known phenomenon that negatively charged dust particles may accumulate near the sheath edges in plasma processing reactors because two opposing forces, ion drag and electrostatic, are in balance.[1–4] Electrostatic forces accelerate the negatively charged dust particles towards the peak in the positive plasma potential, typically near the center of the plasma. Ion drag forces accelerate the dust particles towards the boundaries of the plasma. The forces balance near the sheath edge where the electrostatic force is large. Ion drag forces refer to momentum transfer collisions resulting from Coulomb interactions between a charged species having a large directed velocity and a second charged species. In the case of dust particles, momentum transfer from the positive ion flux, which is directed towards the boundary of the reactor, to the negatively charged dust particles pushes the particles towards those boundaries. The ion drag force scales with the positive ion density which increases with power deposition, whereas the opposing electrostatic force is typically a weak function of power density. The end result is that ion drag forces increase in importance at high power deposition.[4,5]

Ion drag forces in plasma etching reactors also act between the positive ion flux moving towards boundaries and negative ions which are accelerated by the ambipolar field towards the center of the reactor. In typical reactive ion etching (RIE) discharges (ion density $10^9-10^{10}$ cm$^{-3}$, gas pressure 100s mTorr), the positive ion flux is sufficiently small, and the dissipative forces due to ion-neutral collisions (neutral drag) are sufficiently large, that ion drag forces are not important. However, in high plasma density, low gas pressure etching reactors, the larger positive ion fluxes, and lower neutral drag forces, produce conditions where ion drag on negative ions may dominate. In this letter, we discuss conditions in high plasma density etching reactors for which ion drag forces on negative ions are influential in their transport using results from a two-dimensional computer model for plasma equipment. The reactor in this study is an inductively coupled plasma (ICP) etching tool.[6–10] These reactors operate at low gas pressures (<a few to 10s mTorr) and high plasma densities ($>10^{11}-10^{12}$ cm$^{-3}$), conditions which favor ion drag effects.

The model we used in this study has been previously described, and so only improvements will be discussed in detail.[11,12] The simulation, called the Hybrid Plasma Equipment Model (HPEM), is a two-dimensional model consisting of an electromagnetic module (EMM), an electron Monte Carlo simulation (EMCS), and a fluid-chemical kinetics simulation (FKS). The inductively coupled electromagnetic fields are produced by the EMM. Those fields are used in the EMCS to generate the electron energy distribution which are then used to produce electron transport coefficients and electron impact source functions. These values are transferred to the FKS in which the densities for all charged and neutral species are obtained, and Poisson's equation is solved for the electrostatic fields. These densities, conductivities, and fields are then transferred to the EMM and EMCS. This iterative cycle is repeated until a converged solution is obtained.

In the previously described model, ion fluxes were calculated using drift-diffusion relations. In doing so, the ion flux of species $i$, $\mathbf{\Phi}_i$, in electric field $E$ having charge $q_i$, density $N_i$, diffusion coefficient $D_i$ and mobility $\mu_i$, is $\mathbf{\Phi}_i = -D_i \nabla N_i + q_i \mu_i N_i \mathbf{E}$. Here, we have added momentum equations for all ion and neutral species. In doing so, momentum transfer *between* all heavy species is considered. The equations we solve are

$$\frac{\partial N_i}{\partial t} = -\nabla \cdot (N_i \mathbf{v}_i) + \left(\frac{\partial N_i}{\partial t}\right)_c, \tag{1}$$

$$\frac{\partial (N_i \mathbf{v}_i)}{\partial t} = -\frac{1}{m_i}\nabla(kN_iT_i) - \nabla \cdot (N_i \mathbf{v}_i \mathbf{v}_i) + \frac{q_i N_i \mathbf{E}_i}{m_i} - \sum_j \frac{m_j}{m_j + m_i} N_i N_j (\mathbf{v}_i - \mathbf{v}_j)\nu_{ij}. \tag{2}$$

[a]Present address: LAM Research Corp., 4650 Cushing Parkway, Fremont, CA 94538. Electronic mail: wenli.collison@lamrc.com
[b]Author to whom correspondence should be addressed. Electronic mail: mjk@uiuc.edu

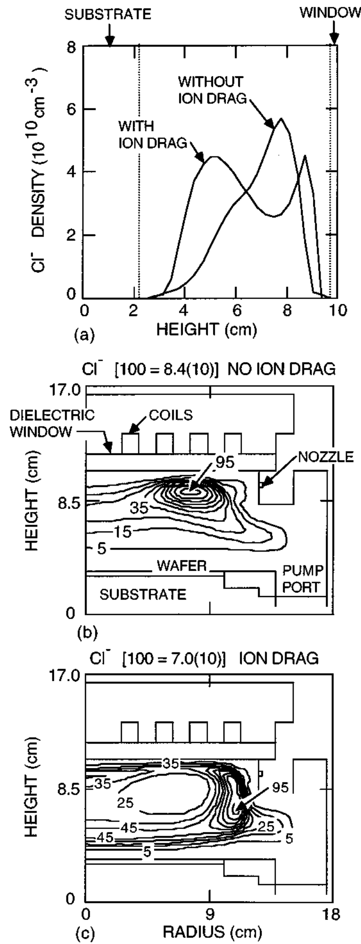


FIG. 1. Densities of Cl $^-$ for a power deposition of 500 W and $T_I = 1500$ K. (a) Cl $^-$ densities as a function of height at a radius of 10 cm with and without the ion drag force. (b) Cl $^-$ densities without ion drag forces. (c) $Cl^-$ densities with ion drag forces. [The contours are labeled with the percentage of the maximum $Cl^-$ density, shown at the top of each figure ($cm^3$)]. Including the ion drag force broadens the $Cl^-$ distribution and forms local extrema near the sheath edges.

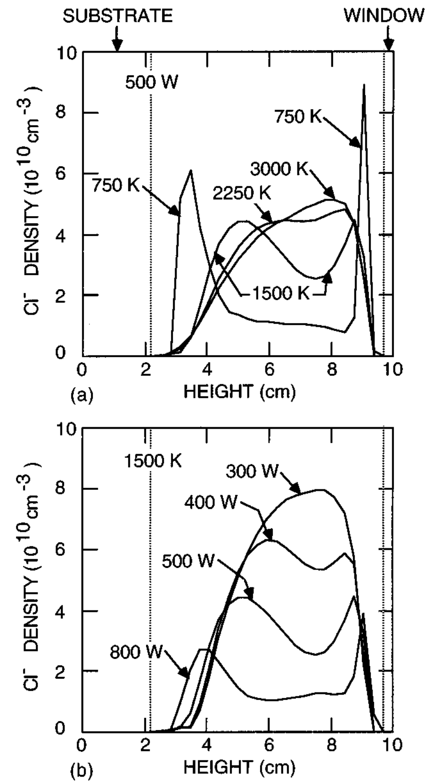


FIG. 2. $Cl^-$ densities as a function of height ($r = 10$ cm). (a) for a power deposition of 500 W for different ion temperatures $T_I$ and (b) for $T_I = 1500$ K for different power deposition. The distributions of $Cl^-$ densities are dominated by ion drag forces at low ion temperature and high power.

In Eqs. (1) and (2), $\mathbf{v}_i$ is the species velocity, $m_i$ is its mass, $T_i$ is its temperature, and $(\partial N_i/\partial t)_c$ is the change in density due to all collisions. $\nu_{ij}$ is the momentum collision frequency between species $i$ and $j$. Slip boundary conditions are used. The sum in Eq. (2) is over all charged and neutral species. Momentum transfer is considered to be conservative and due to isotropic collisions. Momentum transfer collisions between charged species constitute the ion drag force. The input flux of feed stock gases at nozzles, and output flux of products at the pump port are specified as boundary conditions. The density of electrons is still obtained using drift-diffusion techniques to retain a semi-implicit algorithm for solving Poisson's equation.

The momentum transfer cross section due to elastic Coulomb collisions between species $i$ and $j$, which constitute the ion drag force, is $\sigma_{ij} = 5.85 \times 10^{-6} \ln\Lambda/\Psi_{ij}^2 \mathrm{cm}^2$, where $\Psi_{ij}$ is an effective interparticle ion temperature (K), and ln $\Lambda$ is the Coulomb logarithm.[13] $\sigma_{ij}$ scales inversely with the square of the ion energy, and so ion drag effects are particularly sensitive to the total ion energy. In low pressure plasma etching reactors, the directed speed of positive ions can be commensurate with the thermal speed. To account for the directed component of the ion energy in the Coulomb cross section, we use an effective ion temperature

$$\tfrac{3}{2} k \Psi_{ij} = \tfrac{3}{2} k T_I + \tfrac{1}{2} \eta_{ij} |\mathbf{v}_i - \mathbf{v}_j|^2, \quad (3)$$

where $T_I$ is the thermal ion temperature and $\eta_{ij}$ is the reduced mass. This form is often used to characterize ion energies in swarm experiments.[14] $\Psi_{ij}$ increases, and $\sigma_{ij}$ decreases, towards the boundaries where ambipolar forces accelerate ions to high speeds. $\sigma_{ij}$ is about $10^5$ A$^2$ at $\Psi_{ij} \approx 1500$ K, which is much larger than either the ion-neutral momentum transfer cross sections (10–100s A$^2$),[14] or the ion-ion neutralization cross section ($10^3$–$10^4$ A$^2$).[15]

The ICP geometry used in this study is shown in Fig. 1, and is described in detail in Ref. 11. The spiral coil is driven at a frequency of 13.56 MHz and produces a power deposition in the plasma of 500 W unless noted otherwise. The input gas flow is $Ar/Cl_2 = 50/50$ at 100 sccm and a pressure of 10 mTorr. Although the neutral gas temperature is often higher than ambient, we have specified that it be 300 K. The reaction chemistry is the same as described in Ref. 11 with the exception that $SiCl_2$ is the etch product. The positive ions in the simulation are $Ar^+$, $Cl^+$, $Cl_2^+$, $SiCl^+$, and $SiCl_2^+$. The negative ion is $Cl^-$. We have specified the value of $T_I$, and assume it to be constant throughout the reactor.

The predicted $Cl^-$ density is shown in Fig. 1 with and without ion drag forces for $T_I = 1500$ K. The peak total positive ion density in each case is $4.5 \times 10^{11}$ cm$^{-3}$. The maximum positive ion flux is $5.3 \times 10^{16}$ cm$^{-2}$ s$^{-1}$ entering the

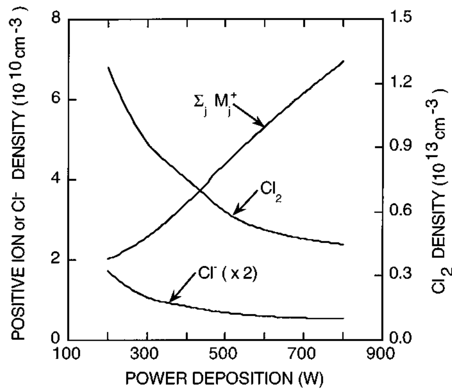


FIG. 3. Total positive ion density ($Ar^+$,$Cl^+$,$Cl_2^+$,$SiCl_+^2$), $Cl_2$ density, and $Cl^-$ density as a function of power deposition. The positive ion density scales nearly linearly with the power deposition. The $Cl^-$ density decreases with increasing power deposition due to the decrease in the $Cl_2$ density.

sheath below the dielectric window at radius of ≈8 cm. The $Cl^-$ density has peak values of $7-8\times10^{10}$ cm$^{-3}$. The low $Cl^-$ density is due, in part, to significant dissociation of the $Cl_2$ feedstock gas. ($Cl^-$ is produced by dissociative attachment to $Cl_2$). In the absence of ion drag forces, the $Cl^-$ density peaks at approximately the midradius where the electrostatic potential is most positive. When including the ion drag forces, the $Cl^-$ density has a local minimum in the bulk plasma and peaks near each sheath edge. The ion drag force is sufficient to overcome the electrostatic force in the bulk plasma where $E$ is small, however, it is not sufficient to overcome the higher electrostatic forces in the sheaths where $E$ is large. The ion drag cross section is also smaller close to the boundaries due to the increase in the ions' directed energy. In fact, the ion drag force does decrease below the electrostatic forces near the boundary but inertia continues to carry negative ions outward. There are no significant changes in the positive ion densities, due to the ion drag force. Charge neutrality is maintained by reapportionment of the electron density.

The densities of $Cl^-$ at a radius of ≈10 cm are shown in Fig. 2(a) for different ion temperatures $T_I$. At high ion temperatures (many 1000 s K), the Coulomb cross sections and ion drag forces are sufficiently small that the electrostatic forces dominate. Ions accumulate near the peak of the plasma potential, albeit with a broader distribution than in the absence of the ion drag forces. As the ion temperature decreases and the Coulomb cross section increases, the $Cl^-$ density extends closer to the walls (and sheaths), indicating an increase in the ion drag forces. At low ion temperatures, the $Cl^-$ density has peaks near the sheaths, similar to those observed for dust particles. The effect is strongest near the window where the positive ion flux is the highest.

Axial $Cl^-$ densities are shown in Fig. 2(b) for an ion temperature $T_I$=1500 K and ICP power depositions of 300–800 W. Over this range of power deposition, the total positive ion densities and ion fluxes increase nearly linearly with power, as shown in Fig. 3. The increased rate of dissociation of the feedstock gases, however, result in a decrease in the density of $Cl_2$, and ultimately in the density of $Cl^-$. At low power deposition (<350 W) and low ion fluxes, the $Cl^-$ density is maximum near the peak in the plasma potential due to the small ion drag forces. At high power deposition and large ion drag forces, the $Cl^-$ density has peaks near the sheath edge.

Radial ion energies have been obtained from observations of Doppler broadened $Ar^+$ optical emission in ICP discharges by O'Neill *et al.*[16] These values varied from 0.08 to 0.25 eV (620–1930 K) over a pressure range of 13–0.18 mTorr. Zheng *et al.*[17] have also inferred the temperatures of ions entering the sheath from etching profiles obtained in ICP discharges, and predict values of 2000–4000 K. At the low end of these ranges, ion drag effects on negative ions are likely to be important. At the high end of these ranges, the ion drag effects are not dominant, but do contribute to spatial broadening of the negative ion densities.

In conclusion, we have investigated the ion drag force on negative ions in ICP reactors using a two-dimensional computer model. At high power deposition (large positive ion fluxes) and low ion temperatures, the ion drag forces are sufficiently large that the negative ion densities are perturbed and, in extreme cases, peak near the sheath edges. This work was supported by Sandia National Laboratory/Sematech, the Semiconductor Research Corp., the National Science Foundation (ECS 94-04133, CTS 94-12565), and the University of Wisconsin ERC for Plasma Aided Manufacturing.

[1] G. S. Selwyn, J. S. McKillop, K. L. Haller, and J. J. Wu, J. Vac. Sci. Technol. A **8**, 1726 (1990).
[2] J. E. Daughtery, R. K. Porteous, M. D. Kilgore, and D. B. Graves, J. Appl. Phys. **72**, 3934 (1992).
[3] M. D. Kilgore, J. E. Daughtery, R. K. Porteous, and D. B. Graves, J. Appl. Phys. **73**, 7195 (1993).
[4] S. J. Choi, P. L. G. Ventzek, R. J. Hoekstra, and M. J. Kushner, Plasma Sources Sci. Technol. **3**, 418 (1994).
[5] D. B. Graves, J. E. Daugherty, M. D. Kilgore, and R. K. Porteus, Plasma Sources Sci. Technol. **3**, 433 (1994).
[6] J. Hopwood, Plasma Sources Sci. Technol. **1**, 109 (1992).
[7] J. H. Keller, J. C. Forster, and M. S. Barnes, J. Vac. Sci. Technol. A **11**, 2487 (1993).
[8] M. S. Barnes, J. C. Forster, and J. H. Keller, Appl. Phys. Lett. **62**, 2622 (1993).
[9] R. Patrick, R. Schoenborn, and H. Toda, J. Vac. Sci. Technol. A **11**, 1296 (1993).
[10] J. B. Carter, J. P. Holland, E. Peltzer, B. Richardson, E. Bogle, H. T. Nguyen, Y. Melaku, D. Gates, and M. Ben-Dor, J. Vac. Sci. Technol. B **11**, 1301 (1993).
[11] P. L. G. Ventzek, M. J. Grapperhaus, and M. J. Kushner, J. Vac. Sci. Technol. B **12**, 3118 (1994).
[12] R. J. Hoekstra and M. J. Kushner, J. Appl. Phys. **77**, 3668 (1995).
[13] M. Mitchner and C. H. Kruger, *Partially Ionized Gases* (Wiley, New York, 1973), Chap. 2.
[14] H. W. Ellis, R. Y. Pai, and E. W. McDaniel, At. Data Nucl. Data Tables **17**, 177 (1976).
[15] R. E. Olson, J. R. Petterson, and J. Moseley, J. Chem. Phys. **53**, 3391 (1970).
[16] J. A. O'Neill, M. S. Barnes, and J. H. Keller, J. Appl. Phys. **73**, 1621 (1993).
[17] J. Zheng, R. P. Brinkman, and J. P. McVittie, J. Vac. Sci. Technol. A **13**, 859 (1995).